Extrapolation from High Enthalpy Tests to Flight Based on the Concept of Local Heat Transfer Simulation

A.F. Kolesnikov
Institute for Problems in Mechanics RAS
Prospect Vernadskogo 101/1
117526, Moscow
Russia

Summary

The concept of the local heat transfer simulation (LHTS) of the high enthalpy flow action on a vehicle stagnation point formulated in refs. 1, 2 is based on the requirement to locally provide in a ground test the same boundary layer on the model at the stagnation point as at the re-entry conditions. The present methodology of the extrapolation from ground to flight consists of the three main parts: 1) the recalculation of the test conditions to flight parameters, 2) the prediction of the test conditions for the given hypersonic flight parameters and 3) the validation of the extrapolation procedure.

The application and validation of this concept are carried out through the comparative analysis of the computed heat transfer rates and profiles of the gas temperature and atoms fractions within boundary layers near the model in the subsonic high enthalpy air flow and near the blunt body in the hypersonic air flow, whose parameters are extrapolated from the inductively heated air plasma experiment. It is established that the LHTS concept provides an excellent accuracy if air temperatures at the outer edges of both boundary layers near a model and a body are close to equilibrium values, or if the surface has a high or moderate catalycity.

The algorithm of determination of the trajectory point for which the complete local duplication of the heat transfer is possible is presented. Another examples of the LHTS concept applications are shown through an analysis of the capabilities of the IPG-4 plasmatron for thermochemical simulation at the Mars probe entry conditions, and through the prediction of the plasmatron subsonic test parameters for the duplication of the stagnation point heat transfer to the Mars Pathfinder aeroshell at the peak-heating conditions in the Martian atmosphere. The computed stagnation point heat flux range for the model in the subsonic dissociated carbon dioxide flow in the whole range of surface catalycity is found in sufficient agreement with the viscous-shock layer analysis carried out in ref. 3 for the Mars Pathfinder aeroshell without the surface ablation.

1. Introduction

In fact, only partial heat transfer simulation for atmospheric entry conditions could be achieved by using high enthalpy wind tunnels [ref. 4]. The stagnation point configuration is most important for the TPM samples testing and surface catalycity rebuilding [refs. 5-14]. In particular, the catalytic properties of the TPM for the Buran space vehicle were studied by using the inductive plasmatron IPG-2 on cylindrical models of the 30 mm in diameter with a flat face [ref. 7]. In subsonic high-enthalpy flows of dissociated nitrogen, oxygen and air, the effective probabilities $\gamma_{WN,O}$ of the catalytic recombination of the N and O atoms on the ceramic tile coating and the antioxidation coating of the carbon-carbon material were determined at the enthalpy 20-22 MJ/kg in the pressure range 0.1-0.3 atm and the surface temperature up to 1750 K: it was found that for the tile surface $\gamma_{WN,O} \leq 3 \cdot 10^{-3}$, for the antioxidation coating of the C-C material $\gamma_{WN,O} \approx 7 \cdot 10^{-3}$ [refs. 2, 7]. Those ground data were completely confirmed by the Bor and Buran space vehicles flight experiments [refs. 15, 16].

The first data on catalytic efficiencies of quartz-based materials and C-C materials have been recently predicted from heat transfer tests in dissociated carbon dioxide flows performed by using the 100-kW inductive plasmatron IPG-4 in subsonic regimes [refs. 12-14]. The question appears how we can extrapolate those data for entry conditions in the Martain atmosphere?

It is almost obvious now that the requirements to duplicate in tests only full-scale values of stagnation pressure and surface temperature [ref. 9] or total enthalpy [ref. 10] are insufficient for the complete simulation of the heat transfer and oxidation and we still need to answer the key question: for what hypersonic flight conditions can we substantially use the ground tests data on the TPM catalytic properties or thermo-chemical resistance for the prediction of the full-scale heat transfer or vehicle surface aging?

For the case of the stagnation point heat transfer (most important from the practical point of view) this question can be solved on the basis of the LHTS concept formulated in refs. 1, 2. This concept includes the requirements to provide in high-enthalpy tests the same values of the total enthalpy, the stagnation pressure and the velocity gradient at the stagnation point of the model as in a hypersonic flow around the vehicle at the given reentry trajectory point. By means of this rather simple theory the ground test data could be extrapolated to flight conditions if we know flow fields around a model and a body (practically - effective radii of a model and a body

Paper presented at the RTO AVT Course on "Measurement Techniques for High Enthalpy and Plasma Flows", held in Rhode-Saint-Genèse, Belgium, 25-29 October 1999, and published in RTO EN-8.

nose). Undoubtedly, an accuracy of such extrapolation should be estimated.

In this paper some results of application and validation of this concept are presented. The validation is carried out through the direct comparison of the numerical solutions of the 1D boundary layer problem for the high-enthalpy experiment and the corresponding 1D thin shock layer problem for the extrapolated flight parameters. The well documented experimental and numerical results for subsonic high enthalpy air flow parameters in the inductive plasmatron IPG-2 [ref. 2] are used.

By means of the LHTS theory the test parameters are recalculated to hypersonic flight conditions and then the nonequilibrium boundary layer near the model and the shock layer near the body along the stagnation line are computed for a 5-species dissociated air. Then stagnation point heat fluxes, temperature and the profiles of *N* and *O* atoms mass fractions within two boundary layers are compared.

It is shown that the surface catalycity and the displacement of air temperature from the equilibrium values at the outer edges of boundary layers are the factors in the actual accuracy of the presented test-to-flight extrapolation.

The algorithm of the determination of the trajectory point for which the local thermochemical simulation could be realized by using plasmatron is described. Two another examples of the applications of the LHTS concept are demonstrated through analysis of the Mars probe trajectory [ref. 17] and test parameters required for the stagnation point heat transfer simulation for the Mars probe and the Mars Pathfinder aeroshell at the trajectory peak-heating point in the Martian atmosphere [ref. 3] by using the 100-kW inductive plasmatron IPG-4 [refs. 11-14] and the standard European model configuration [refs. 9, 12-14]. The numerically predicted heat transfer range for the experiment in a subsonic high-enthalpy carbon dioxide flow is found in good agreement with computations for the Mars Pathfinder aeroshell from ref. 3 in the whole range of the surface catalycity.

2. Concept of the Local Heat Transfer Simulation

Our way to study the problem of the ground-to-flight extrapolation lies in the use of the theory of the local heat transfer simulation formulated in refs. 1, 2. At least for the case of the stagnation point heat transfer we can point out the hypersonic flow parameters and a blunt body radius which are in direct correspondence with high enthalpy subsonic flow parameters and a model radius (*Fig. 1*) if both surfaces have the same catalycity and emissivity and also the same heat transfer boundary conditions (for example, radiative-equilibrium walls).

The analysis is based on the boundary layer theory for dissociated reacting gases. Fay and Riddell theory [ref. 18] gives the following expression for the heat flux at the

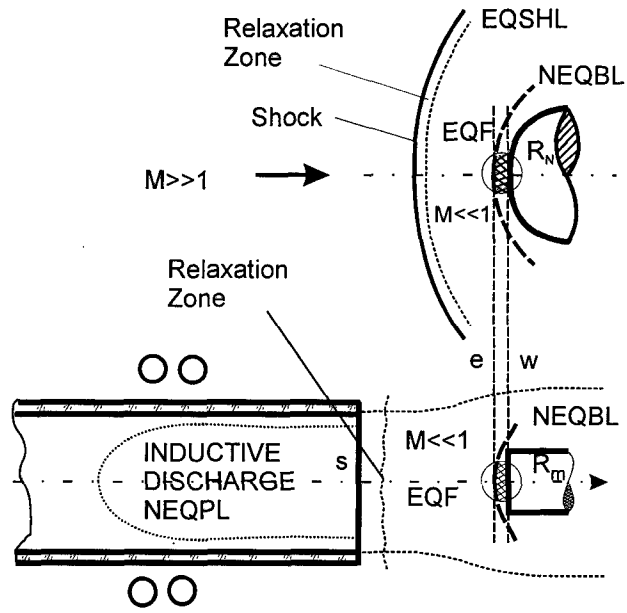

Fig. 1. Schemes of hypersonic flow around a blunt body and the stagnation point heat transfer simulation in subsonic high enthalpy flow in plasmatron.

stagnation point of a blunt body with a fully catalytic surface which is being flown by a hypersonic flow:

$$q_W = 0.763\, Pr^{-0.6}(\rho_e\mu_e)^{1/2}\left(\frac{dU_e}{ds}\right)_0^{1/2}\left(\frac{\rho_W\mu_W}{\rho_e\mu_e}\right)^{0.1}\times \quad (2.1)$$
$$\times(h_e - h_W)$$

For the case of the frozen boundary layer the Goulard's solution of the boundary layer problem [ref. 19] gives the following formula for the stagnation point heat flux to the wall with arbitrary catalycity:

$$q_W = 0.66\, Pr^{-2/3}(\rho_e\mu_e)^{1/2}\left(\frac{dU_e}{ds}\right)_0^{1/2}(H_e - h_W)[1+$$
$$+(Le^{2/3}\Phi - 1)\frac{h_A^0(c_e - c_W)}{H_e - h_W}], \quad (2.2)$$
$$\Phi = \left(1+\frac{0.47Sm^{-2/3}(2(dU_e/ds)_0\rho_e\mu_e)^{1/2}}{\rho_W k_W}\right)^{-1}$$

Here H is the total enthalpy, h is the enthalpy, h_A^0 is the enthalpy of formation of atoms, c is the mass fraction of atoms, ρ is the density, μ is the viscosity, $(dU_e/ds)_0$ is the velocity gradient, Pr is the Prandtl number, Le the Lewis number, Sm is the Schmidt number. The subscripts e and w denote the outer edge of the boundary layer and the body surface, respectively.

The analysis of the formulae (2.1) and (2.2) has revealed the three independent factors which control the heat flux: H_e-h_W, ρ_e and $(dU_e/ds)_0$. In the case when the flow at the outer edge of the boundary layer is in equilibrium, ρ_e is the function of $h_e(=H_e)$ and p_e, and accordingly to

Goulard's solution [ref. 19] h_W appears to be a parameter dependent on h_e, p_e, $(dU_e/ds)_0$ and T_W. Therefore, the stagnation point heat flux q_W is completely determined by the boundary condition on the body and the three parameters at the outer edge of the boundary layer: the enthalpy, the stagnation pressure and the velocity gradient.

We see, that the sufficient conditions of equality of the heat fluxes in flight and in ground test are the equalities of these three parameters in the two flows:

$$H_S=H_\infty,\ p_{eS}=p_{e\infty}=p_W,\ (dU_e/ds)_{0S}=(dU_e/ds)_{0\infty} \quad (2.3)$$

where the subscripts ∞ and S relate to the flight and ground conditions.

Let's consider the conditions of duplication of the stagnation point heat transfer to a blunted body of radius R_W, which is being flown by a hypersonic flow with velocity V_∞ and density ρ_∞, in an axisymmetric high enthalpy subsonic flow with velocity V_S and static pressure p_S by using a cylindrical blunted model of radius R_m (*Fig. 1*).

From the first equality (2.3) the equality of the total enthalpies of the two flows follows:

$$\frac{1}{2}V_S^2+h_S=H_\infty \quad (2.4)$$

The second necessary condition reduces to the relation between the static pressure of the free stream in a plasma wind tunnel and the given stagnation pressure p_W, which is described by the approximate Poisson's adiabat equation for a real gas [ref. 20]:

$$p_S\left(1+\frac{\gamma_{*S}-1}{2}M_S^2\right)^{\gamma_{*S}/(\gamma_{*S}-1)}=p_W, \quad (2.5)$$

$$\gamma_{*S}=\frac{1}{1-p_S/\rho_S h_S}$$

where γ_{*S} is the effective specific heat ratio, and $M_S<1$ is the Mach number of the simulating flow.

Let's represent the third condition - the equality of the stagnation point gradients - in the form

$$V_S/R_m^*=V_\infty/R_N^*, \quad (2.6)$$

$$R_{m,N}^*=V_{S,\infty}/(dU_e/ds)_{0S,\infty}$$

where R_m^* and R_N^* are the effective radii of the model and the body at the stagnation points. Assuming the parameters V_∞, H_∞, p_W, R_m^*, and R_N^* to be known from (2.4)-(2.5) we obtain the parameters of the ground free stream in the following form:

$$V_S/V_\infty=\xi,\ h_S/H_\infty=1-\zeta^2, \quad (2.7)$$

$$p_S/p_W=(1-\zeta^2)^{\gamma_{*S}/(\gamma_{*S}-1)}, \quad (2.8)$$

$$M_S^2=\frac{2}{(\gamma_{*S}-1)}\frac{\zeta^2}{1-\zeta^2}, \quad (2.9)$$

$$\xi=R_m^*/R_N^*,\ \zeta=(V_\infty^2/2H_\infty)\xi^2, \quad (2.10)$$

$$\xi\le\frac{\sqrt{2H_\infty}}{V_\infty}\zeta_*,\ \zeta\le\zeta_*=\sqrt{\frac{\gamma_{*S}-1}{\gamma_{*S}+1}}$$

The expressions for calculating the velocity, enthalpy, pressure and Mach number of the simulating flow (2.7) are universal in form: they contain only two dimensionless parameters ξ and ζ. For the hypersonic flight in an atmosphere $V_\infty^2/2H_\infty\cong 1$, then $\xi=\zeta$.

Thus, for high-enthalpy flows in which the stagnation point heat fluxes at the body and the model are equal, the ratios V_S/V_∞ and h_S/H_∞ are completely determined by the elementary universal relations (2.7). The relations (2.8) and (2.9) for high-enthalpy flows are the universal implicit relations of the functions $p_S'(\zeta)=p_S(\zeta)/p_W$ and $M_S(\zeta)$, since γ_{*S} depends on the values of p_S and h_S.. In *Fig. 2* we have plotted the functions $p_S'(\zeta)$ and $M_S(\zeta)$ calculated for equilibrium air at H_∞=32 (*a*), 16 (*b*) and 8 (*c*) MJ/kg. The curves *1-3* correspond to $p_W=10^{-3}$, 1 and 10^2 atm. The broken curves correspond to a perfect gas with constant γ=1.4.

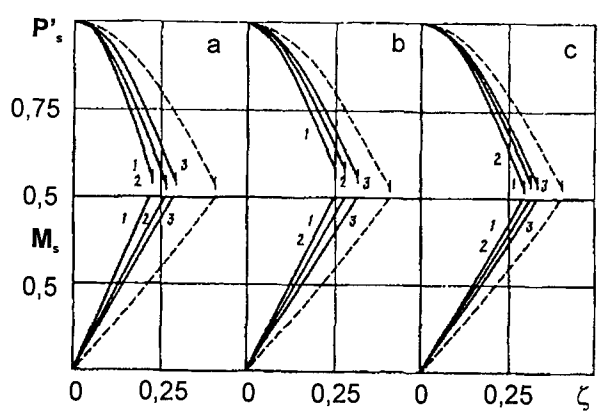

Fig. 2. Universal dependencies of the dimensionless static pressure and Mach number of simulating subsonic air flow versus similarity parameter ζ [ref. 1].

As may be seen from *Fig. 2*, the real properties of highly dissociated air essentially affect the functions

$p_S'(\zeta)$ and $M_S(\zeta)$, which are quite important for the analysis of the test conditions.

3. Recalculation of Test Parameters to Flight Conditions

For the experimental practice of the heat transfer simulation the case $\zeta<<1$ is very important: practically, this case occurs when $R_m<<R_N$. Let's consider this case in detail taking into consideration that for a hypersonic axially symmetric flow around a smooth blunted body we have the following well-known formulae (ref. 20):

$$H_\infty = \frac{1}{2}V_\infty^2, \quad p_W = \rho_\infty V_\infty^2, \tag{3.1}$$

$$\left(\frac{dU_e}{ds}\right)_0 = \left(\frac{8}{3}\frac{\rho_\infty}{\rho_e}\right)^{\frac{1}{2}} \frac{V_\infty}{R_N} \tag{3.2}$$

Then for the ground subsonic free stream conditions we have:

$$h_S = \frac{1}{2}V_\infty^2, \quad p_S = \rho_\infty V_\infty^2, \tag{3.3}$$

$$V_S = \left(\frac{8}{3}\frac{\rho_\infty}{\rho_e}\right)^{1/2} \frac{R_m^*}{R_N} V_\infty \tag{3.4}$$

In the case of subsonic jet the subscript S denotes the center of the flow.

The conditions (3.3) are rather simple, but the condition (3.4) is not trivial and contains the geometrical parameter - effective radius R_m^*, which depends on the channel radius R_c, the model radius R_m and should be computed for the test configuration by using CFD methods. For subsonic jets over cylindrical models with a flat face we obtained the following approximation for R_m^* from numerical solutions of the Navier-Stokes equations [ref. 1]

$$R_m^* = \begin{cases} R_m\left[2 - l - 1{,}68(l-1)^2 - 1{,}28(l-1)^3\right], & l \le 1 \\ R_c, \quad l > 1 \quad (l = R_m / R_c) \end{cases} \tag{3.5}$$

In accordance with (3.3), (3.4) there is one-to-one correspondence between subsonic jet parameters $h_S, p_s(\approx p_W), V_S$ and the given dimensions R_C and R_m, on the one hand, and the parameters of the hypersonic flow and the nose radius of a blunt body, on the other

$$V_\infty = \sqrt{2h_S}, \quad \rho_\infty = \frac{p_S}{2h_s}, \tag{3.6}$$

$$R_N = \left(\frac{8}{3}\frac{\rho_\infty}{\rho_e}\right)^{1/2} \frac{V_\infty}{V_s} R_m^*$$

As an example, let's analyze the well characterized subsonic regime performed in the IPG-2 plasmatron for the air flow at the pressure 0.1 atm , the generator anode power 37.4 kW and the mass flow rate through the discharge channel 2.8g/s [ref. 2]. At the distance of 30 mm from the plasmatron exit section, the enthalpy $H_e=2.19\cdot10^7$ m^2/s^2 , the velocity V_s=180 m/s, the density $\rho_s=3.86\ 10^{-3}$ kg/m^3, Reynolds number $Re_s=\rho_s V_s R_m/\mu_s \cong$ $\cong$58.6, Mach number M_S=0.14. The radius of the IPG-2 plasmatron channel $R_c=3\cdot10^{-2}$ m and for the cylindrical model of the radius $R_m=1.5\cdot10^{-2}$ m we have $R_m^*=1.2R_m=1.8\cdot10^{-2}$ m, in accordance with (3.5).

For these subsonic air flow parameters we have determined the parameters of the hypersonic air flow and the nose radius of a blunt body from expressions (3.6): V_∞=6620 m/s, $\rho_\infty=2.28\cdot10^{-4}$ kg/m^3, R_N= 0.265 m. The density value corresponds to the altitude 62.4 km in the Earth atmosphere. Correspondingly, the flight Reynolds number Re_∞=1750 and the Mach number M_∞=20. We see, that Reynolds and Mach numbers are quite different for those ground test and hypothetical flight regime. That means that Reynolds and Mach numbers are not the similarity parameters for the stagnation point heat transfer.

4. Method of the LHTS Concept Validation

The proposed method of the LHTS concept validation consists in the direct comparison of the calculated heat transfer rates and the profiles of the temperature and species fractions within the boundary layers near the stagnation points of the model and the body for subsonic and hypersonic flows conditions linked by the correlation (3.6). Such a comparison is carried out below.

A method for the calculation of the heat transfer rates at the stagnation point of a model with a flat face exposed to a subsonic jet of a viscous multicomponent reacting gas was developed in refs. 2, 7, 21, 22, 13. Here we also use the concept of a boundary layer with finite thickness in the vicinity of the stagnation point. The thickness δ of the boundary layer and the hydrodynamic parameters at its outer edge, including the flow vorticity, which are given below in the formulation of the problem, are determined from the numerical solution of the full Navier-Stokes equations, which is considered as an outer solution.

In the case of a one-temperature multicomponent mixture of atoms and molecules in the equilibrium excitation of the vibrational degrees of freedom, the system of the ordinary differential equations describing the flow within the boundary layer near the stagnation point of the model has the following form (ref. 21):

$$\left(l u'_\eta\right)'_\eta + f u'_\eta - \frac{u^2}{2} + \frac{1+\alpha_e}{2\rho} = 0, \qquad (4.1)$$

$$\left(\frac{l}{Pr} H'_\eta\right)'_\eta + f H'_\eta + \left[\frac{l}{Pr}\sum_{i=1}^{N}(h_i - h_i)^*(Le_i - 1)c'_{i\,\eta}\right]'_\eta = 0,$$

$$\left(\frac{l}{Sc_i} c'_{i\eta}\right)'_\eta + f c'_{i\eta} + w_i = 0\ (i = 1,\ldots < N - N_e),$$

$$f'_\eta = u, \quad y'_\eta = \Delta_\rho^{-1}\chi^{-1}, \quad 1/\rho = T/m,$$

$$c_j^\bullet \equiv c_{j_e}^\bullet, \quad J_j^\bullet \equiv 0 (j = 1,\ldots,N_e), \quad H = \sum_{i=1}^{N} c_i h_i,$$

$$l = \frac{\mu\rho}{\eta_e^2}, \quad \eta_e = \frac{\Delta}{\chi}\sqrt{2 Re u_{1e}}, \quad \chi = \int_0^1 \frac{d\eta}{\rho}, \quad Re = \frac{\rho_S V_S R_m}{\mu_e},$$

$$\Delta = \delta / R_m, \quad u = u_1 / u_{1e}, \quad u_1 = \partial u / \partial x, \quad \upsilon = -V^0 / V_s,$$

$$\alpha_e = -\upsilon_e (\partial u_1 / \partial y)_e / u_{1e}^2, \quad U = U^0 / V_s, \quad x = x^0 / R_m,$$

$$y = y^0 / R_m, \quad \rho = \rho^0 / \rho_e, \quad T = T^0 / T_e, \quad h_i = h_i^0 / H_e.$$

The boundary conditions at the outer edge of the boundary layer and on the surface of the model are:

$$\eta = 1: \quad u = H = 1, \quad c_i = c_{i_e}\ (i = 1,\ldots, N - N_e) \qquad (4.2)$$

$$\eta = 0: \quad u = f = 0, \quad T = T_w, \quad y = 0,$$

$$\frac{\mu}{Sc_i \eta_e} c'_{i\eta} = \frac{K_{w_i}}{V_s u_{1e}}\sqrt{\frac{Re u_{1e}}{2}}\, c_i \qquad \left(K_{w_i} = \frac{2\gamma_i}{2-\gamma_i}\sqrt{\frac{kT_w}{2\pi m_i}}\right)$$

In (4.1), (4.2) U^0, V^0 are the velocity components in the cylindrical coordinate system x^0, y^0 which is related with a flat face, ρ is the density, c_i is the mass fraction, h_i is the enthalpy, h_i^* is the energy of formation of the species i; c_j^*, J_j^* are the mass fraction and the diffusive flux of the chemical element j; H is the enthalpy of the gas mixture, T is the temperature, m is the molecular weight, K_{Wi} and γ_i are the effective heterogeneous recombination rate constant and the catalytic efficiency; k is the Boltzmann constant, m_i is the molecular weight of the species i, N is the number of species, N_e is the number of chemical elements, and η is the Dorodnitsyn's variable. The circle superscript denotes dimensional quantities.

In the momentum equation the parameter α_e=const takes into account the vorticity of the flow at the outer edge of a boundary layer of the thickness δ. Parameters α_e, U_e and u_{1e} are determined from the profiles of the velocity components obtained from the numerical solution of the Navier-Stokes problem for a viscous reacting gas jet flow past a cylinder with the flat face at M<<1 [refs. 2, 7, 19].

For our case $\Delta=\delta/R_m$=0.4, υ_e=0.52, u_{1e}=0.445, α_e=2.626. It was assumed in calculation that Pr=0.71, Sc=0.65 and $\mu \sim T^{0.77}$.

We assume that the following gas-phase reactions in a 5-species air occur within the boundary layer: *1)* $O_2+M \leftrightarrow O+O+M$, *2)* $N_2+M \leftrightarrow N+N+M$, *3)* $NO+M \leftrightarrow N+O+M$, *4)* $O+N_2 \leftrightarrow N+NO$, *5)* $O+NO \leftrightarrow N+O_2$. The chemical equilibrium is supposed to be at the outer edge of the boundary layer: p_S=0.1 atm, H_e=2.19·10^7 m^2/s^2, T_e=5960 K, C_{N2}=0.4576, C_{O2}=0.3513·10^{-3}, C_{N2}= 0.2922·10^{-2}, C_N= 0.3091, C_O=0.2304.

The thin viscous shock layer model was used independently for the computation of the hypersonic air flow (V_∞=6620 m/s, ρ_∞=2,28·10^{-4} kg/m^3) past a sphere of the radius R_W=0,265 m. At the formulation of this problem the same boundary conditions at the wall and the same chemical reactions rates, as for the subsonic flow, were used. For the numerical solutions of the problem (4.1), (4.2) and the viscous shock layer problem the fourth-order-accurate finite-difference scheme was used. All computations were made for the surface temperature T_W=1500 K.

5. Results of Validation for Subsonic Air Test

Fig. 3 shows the calculated dependencies of the stagnation point heat fluxes q_W to the model (M<<1) and the body (M>>1) as the functions of the heterogeneous recombination rate constant K_W for the case $K_{WO}=K_{WN}=K_W$ at test and flight conditions specified above.

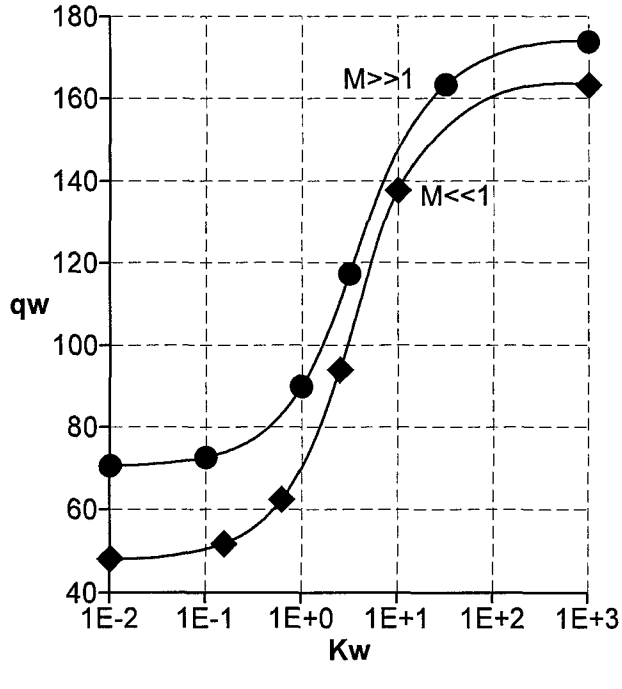

Fig. 3. Stagnation point heat transfer rates q_W,(W/cm^2) versus effective rate constant of surface atom recombination K_W,(m/s) for plasmatron test (M<<1) and extrapolated to flight (M>>1).

For a highly catalytic surface the difference in the heat fluxes q_W under corresponding conditions for the subsonic and the supersonic flows is only about 5%. As K_W decreases, this difference increases and for a noncatalytic surface in the subsonic jet the heat flux is 30% less then the heat flux in the corresponding hypersonic flow.

So, we see, that the accuracy of the heat transfer simulation on the basis of the LHTS theory developed in refs. 1, 2 depends on the surface catalytic efficiency. The accuracy is rather good for surfaces with high and moderate catalycity but it looks insufficient for a noncatalytic one. Nevertheless, both curves in *Fig. 3* are functionally similar and they have the same practically important interval $10^{-1}<K_W< 10^2$ m/s, where the heat transfer rates drastically depend on wall catalycity.

Moreover, it is easy to find by using *Fig. 3* that at least one function exists, which is duplicated with a quite perfect accuracy - the normalized heat flux

$$q_W^* = \frac{q_W - q_{Wn}}{q_{Wk} - q_{Wn}}, \qquad (5.1)$$

where q_{Wk} is the heat flux to a fully catalytic wall and q_{Wn} is the heat flux to a noncatalytic wall.

From here we can conclude that the data on the effective catalytic rates for atomic oxygen and nitrogen recombination on the Buran TPM $1 \le K_W \le 3$ m/s, obtained in subsonic jets [refs. 2, 7, 20], are quite applicable to hypersonic re-entry conditions in the Earth atmosphere with flight parameters of the same orders of magnitude that calculated above.

For the more clear understanding of the LHTS capabilities we will compare the profiles of the air temperature, N and O atoms fractions across the boundary layer near the model and across the shock layer near the body at the same conditions for two limiting cases: fully and noncatalytic walls.

Fig. 4 shows the temperature profiles within the boundary layer near the model and within the shock layer near the blunt body for a fully catalytic wall case. We see that temperature profiles are rather different at the outer edges of two boundary layers. For the hypersonic flow the temperature T_e considerably (~ by 2000 K) exceeds the equilibrium value because the shock layer is fully nonequilibrium in this case, but at the same time the two temperature profiles are quite close to each other near the walls. This leads to good agreement between thermal conductive parts of the heat fluxes to fully catalytic surfaces of the body and the model.

Within the hypersonic shock layer we can see some displacement of the N atoms mass fraction from the equilibrium value at the outer edge of the boundary layer (see *Fig. 5*): the mass fraction c_N is significantly less then the equilibrium value in the subsonic flow. On the other hand, close to fully catalytic surfaces (*Fig. 5*), the profiles of the N atoms fractions for the considered subsonic and hypersonic air flows are quite similar

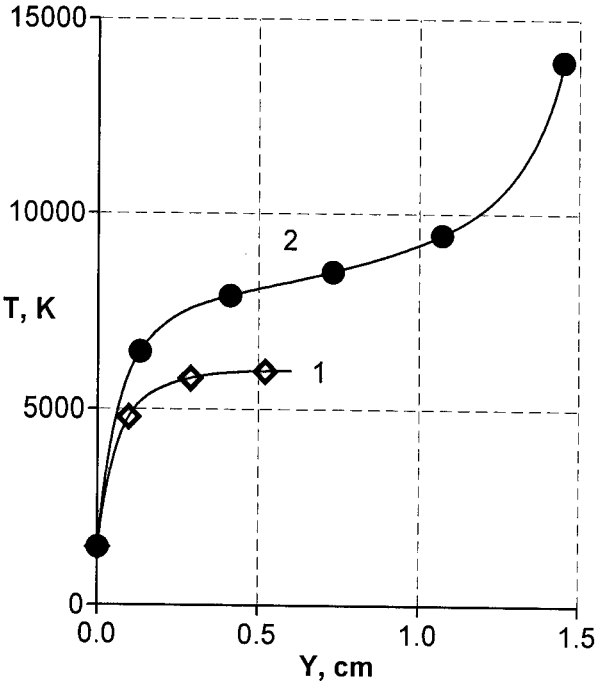

Fig. 4. Temperature profiles along stagnation line (fully catalytic wall): 1 - the boundary layer near the model in subsonic flow (R_m=1.5 10^{-2} m); 2 - the hypersonic shock layer near the body (R_N=0.265 m).

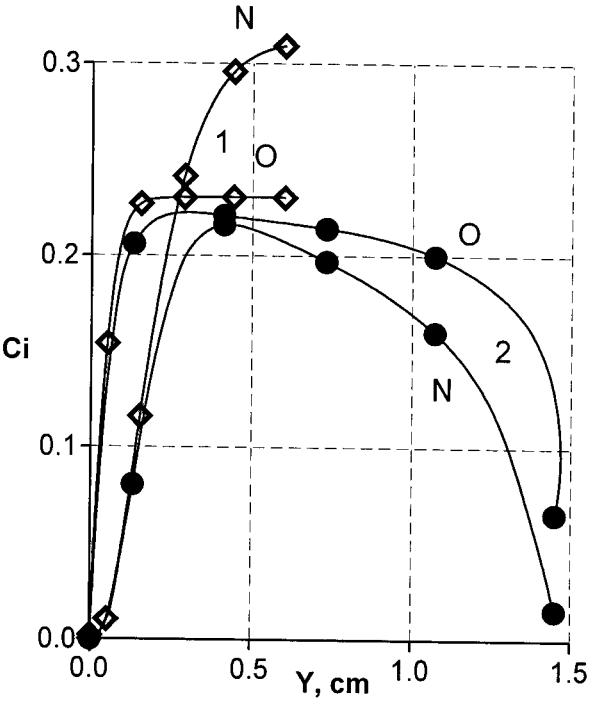

Fig. 5. Profiles of the mass fractions of N and O atoms along stagnation line (fully catalytic wall): 1 - the boundary layer near the model in subsonic flow, 2 - the hypersonic shock layer near the body.

including the fine details of different behavior of the profiles of *N* and *O* atoms due to the exchange reactions in dissociated air and mentioned above in the chapter **4**. In fact, the contributions in the heat fluxes due to nitrogen atoms diffusion are insignificant in this case. Also we can see on *Fig. 5* that the excellent simulation accuracy is achieved for the atomic oxygen fraction profile within the whole boundary layer because oxygen is completely dissociated at the outer edges of both boundary layers. As a result the contributions in the heat fluxes due to the atomic oxygen diffusion for both flows are equal within 5%. The same is correct for the total heat fluxes to a fully catalytic wall.

For the noncatalytic wall case the situation is more dramatic as we can see in *Fig. 6* and *7*. The temperature profiles across boundary layers are different exterior to the nearest vicinities of stagnation points and the heat flux caused by the to thermal conductivity is 30 % higher in the supersonic flow, then in subsonic one.

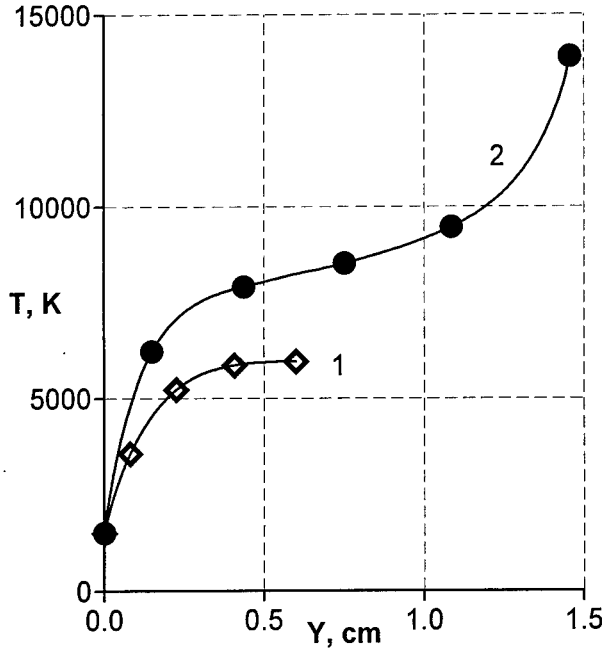

Fig. 6. Temperature profiles along stagnation line (non-catalytic wall): 1 - the boundary layer near the model in subsonic flow, 2 - the hypersonic shock layer near the body.

Both boundary layers are almost frozen and diffusion does not influence heat transfer. The atomic nitrogen fraction near the surface of the model is higher in the plasmatron test, but the atomic oxygen fraction profiles within boundary layers are quite close in test and hypothetical flight (*Fig. 7*). That means the formulae (3.6) for ground-to-flight extrapolation should provide a complete simulation of the diffusion flux and the partial pressure of atomic oxygen and, therefore, surface catalysis and oxidation processes. These are the arguments for using here the term "thermochemical" simulation.

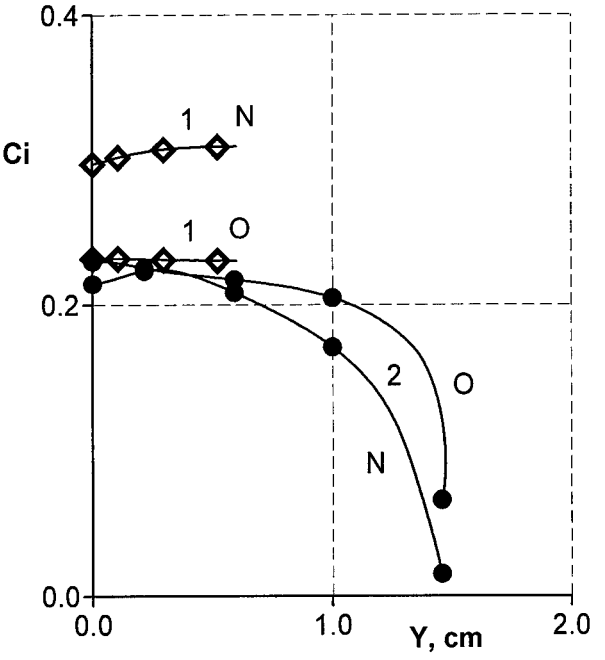

Fig. 7. Profiles of the mass fractions of N and O atoms along stagnation line (noncatalytic wall): 1 - the boundary layer near the model in subsonic flow, 2 - the hypersonic shock layer near the body.

It was established in ref. 23, that an accuracy of the heat transfer duplication for low catalytic surface was improving when the pressure in subsonic high enthalpy flow was increasing. When $p_S \geq 0.2$ atm the difference in the q_W for subsonic and hypersonic flow was not more 5% for surfaces with $K_W \geq 1$ m/s (the quite practical case). The example of the excellent duplication of the temperature distribution across the boundary layer for hypersonic flow conditions we can see on *Fig. 8* for high enthalpy subsonic test in dissociated nitrogen [ref. 23].

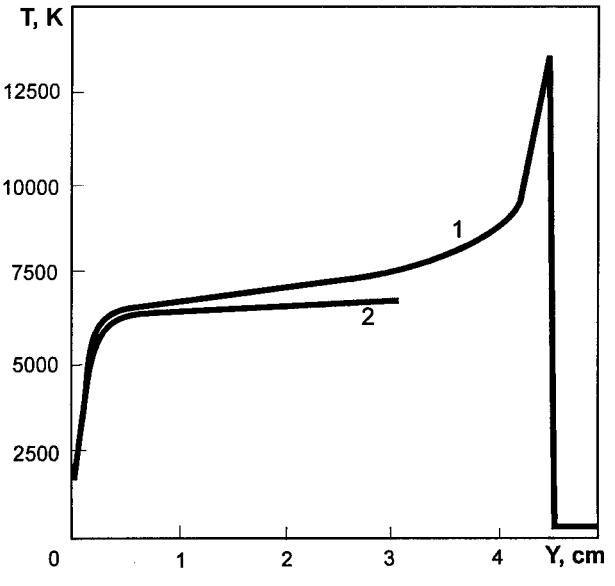

Fig. 8. Temperature distributions along stagnation line in hypersonic shock layer (1: M_∞=20, V_∞=6490 m/s, Z=62 km, R_W=0.95 m) and in subsonic jet (2: M_S=0.04, V_S=50m/s, p_S=0.3 atm, H_S=21 MJ/kg, R_m=1.5·10^{-2}m).

We can conclude that the displacement of air temperature from the equilibrium value at the outer edges of boundary layers in high-enthalpy tests or in flight is a factor in actual accuracy of the LHTS concept. One should expect that the agreement between the heat fluxes and two boundary layer structures will be improved when the air temperatures outside boundary layers are closer to equilibrium, for example, - for higher values of the pressure as has already been predicted for the high-enthalpy nitrogen experiment in ref. 23.

6. The Trajectory Point for the Complete Local Duplication of Heat Transfer

One in the main features of the subsonic high enthalpy jets is the nonuniformity of the enthalpy and velocity profiles at the plasma generator channel exit and the decreasing of these characteristics along the flow axis. In order to take these effects into account, in relations (2.7) instead of V_S and h_S we should, substitute the velocity and enthalpy values on the axis of the free stream corresponding to the distance L from the plasmatron channel exit to the model.

For the modeling in a hyposonic flow ($M<<1$), taking into account the above we can generalize relations (3.3), (3.4) in the following form

$$h_S = \frac{1}{2}\varphi_H^{-1}(L)V_\infty^2, \quad p_S = (1-\kappa)\rho_\infty V_\infty^2, \kappa = \frac{\rho_\infty}{\rho_e} \quad (6.1)$$

$$V_S = \varphi_V^{-1}(L)\left(\frac{8}{3}\kappa\right)^{1/2}\frac{R_m^*}{R_N}V_\infty \quad (6.2)$$

Here, the factors $\varphi_H(L)$ and $\varphi_V(L)$ take into account the decreasing of the enthalpy and velocity along the axis of the free subsonic stream, the subscript S relates to the center of the plasmatron channel exit.

As we mentioned above, the parameters h_S, p_S and V_S are in functional coupling. For a wide range of the subsonic tests conditions in the optimum discharge burning regime these parameters could be presented with a functional relationship

$$p_S V_S = \chi(h_S, Q, p_S) \quad (6.3)$$

where Q is the mass flow rate and $\chi(h_S, Q, p_S)$ is the specific functional characteristic of the plasmatron. This characteristic should be determined for each facility which is used for the heat transfer duplication.

If function χ is known, we can eliminate p_S and V_S in (6.3) using (6.1) and (6.2) and obtain the following relationship between the hypersonic flow parameters ρ_∞ and V_∞

$$\rho_\infty = \left(\frac{8}{3}\kappa\right)^{-1/2}(1-\kappa)^{-1}\varphi_V^{-1}(L)\frac{R_N}{R_m^*}V_\infty^{-3} \times \times\chi\left(\frac{V_\infty^2}{2\varphi_H(L)}, Q, (1-\kappa)\rho_\infty V_\infty^2\right) \quad (6.4)$$

For the following step of the procedure, it is necessary to present the trajectory of the body in the atmosphere in the parametric form $V_\infty = F(\rho_\infty)$. The intersection of this curve with the curve (6.4) in the plane ρ_∞-V_∞, if it exists, gives us the trajectory point for which the complete local heat transfer duplication could be achieved.

For the specified parameters V_∞, ρ_∞, and R_N, the complete local simulation of the heat transfer is possible for the appropriate model (or channel) dimension. In this case the test conditions can be predicted in accordance with the following algorithm. The free stream parameters h_S, p_S, and V_S are calculated from (6.1) and (6.3), and then the effective radius R_m^* is calculated from (6.2). The necessary value of R_m^* is insured by choosing a model or channel with the appropriate geometry (for models with flat face in accordance with expression (3.5)).

7. Analysis of the Mars probe trajectory and Requirements for Plasmatron Tests

Let's apply the LHTS concept in order to estimate the IPG-4 plasmatron capabilities for complete local duplication of the stagnation point heat transfer for the Mars probe trajectory parameters in a subsonic test with carbon dioxide. The IPG-4 operating envelope for the subsonic regime with carbon dioxide as a working gas (*Fig. 9*) contains the peak-heating parts of the Mars probe trajectory [ref. 17].

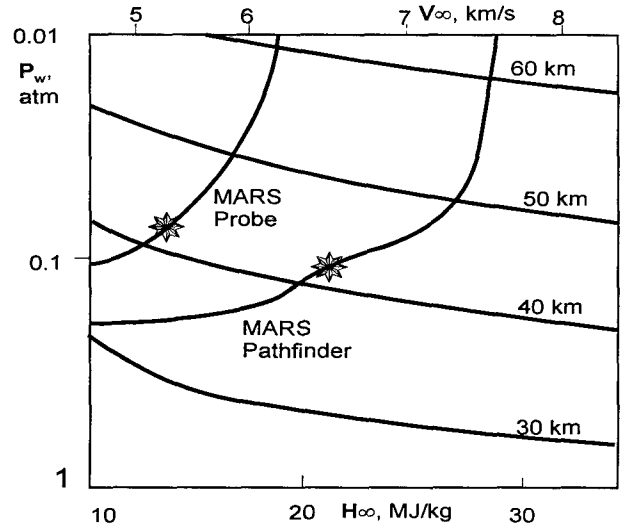

Fig. 9. The IPG-4 operating envelope in the stagnation pressure-enthalpy coordinates for subsonic regime with carbon dioxide, and the Mars Pathfinder and the Mars Probe trajectories; the stars indicate the peak-heating points [ref.24].

The velocity V_∞, the altitude H and the calculated convective heat flux to fully catalytic radiative-equilibrium wall q_w at the stagnation point for the probe with R_N=0.8 m are presented in *Fig. 10* as functions of the entry time [ref. 17].

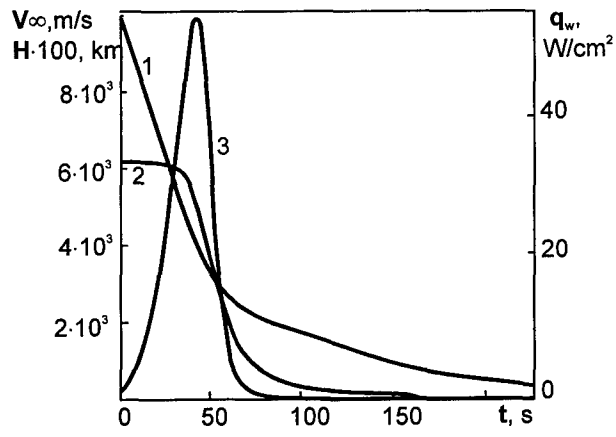

Fig. 10. Mars probe trajectory and convective heat flux at stagnation point to fully catalytic radiative-equilibrium wall (R_N=0.8 m, ε_{th}=0.85) [ref. 24]: 1 - H·100, 2 - V_∞, 3 - q_W.

In accordance with these data and the density distribution in the Martian atmosphere from ref. 17 we have calculated, by using (3.3), the dependencies $p_s(t)$ and $h_s(t)$ that are presented in *Fig. 11* by the curves *1* and *2*. Also, in *Fig. 11* the part of the IPG-4 operating envelope in coordinates p_s-h_s for the carbon dioxide gas is shown.

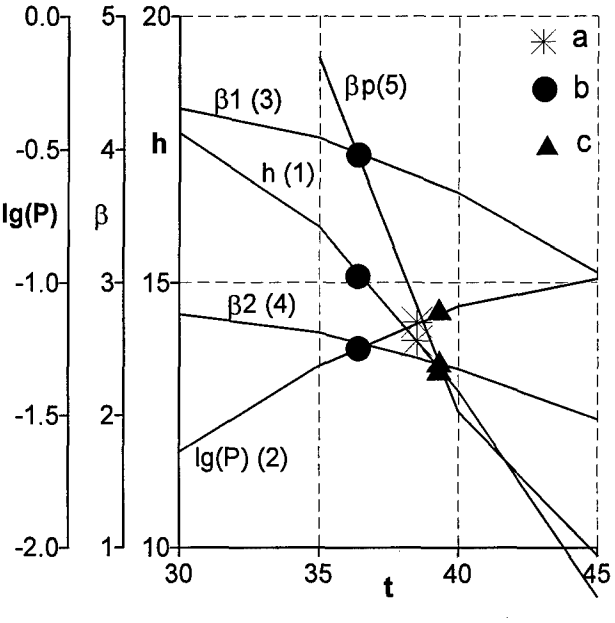

Fig. 11. Heat transfer parameters for the Mars probe within the IPG-4 operating envelope as the functions of the entry time t (sec) [ref. 24]. Curves: 1 - enthalpy (MJ/kg), 2 - normalized stagnation pressure (p0=1 atm), 3, 4 - velocity gradients (10^3 s^{-1}) in hypersonic flow for R_N=0.8 and 1.25 m, 5 - velocity gradient (10^3 s^{-1}) in subsonic jet for the euromodel; points: a - the peak heating point, b and c -the points of the complete thermochemical simulation.

We see, that the IPG-4 envelope contains the both curves $p_s(t)$ and $h_s(t)$ within the entry time interval 25≤t≤44 s. This interval includes the heat-intensive part of the probe trajectory during the period 30≤t≤44 s (*Fig. 10*). The maximum value of a heat flux should be achieved at the point t^*=38.5 s where Z=43.0 km and V_∞^*=5995 m/s. One could expect that for an accurate simulation the heat transfer at that most important trajectory point it is necessary to have the subsonic flow in the IPG-4 with the enthalpy h_s^*=14.02 MJ/kg and the static pressure p_s^*=6.7·10^{-2} atm.

Taking into account, that in the IPG-4 subsonic regimes the pressure p_s and the enthalpy h_s could be controlled independently by using the vacuum pump system and by the variation of energy input in plasma [refs. 12-14], from *Fig. 11* we can conclude that it is possible to duplicate simultaneously both functions $p_s(t)$ and $h_s(t)$ in the real time scale during 19 seconds.

But in fact this way of the duplication of only two heat transfer parameters would not be the complete simulation of heat transfer because the satisfaction of conditions (3.3) does not guarantee the satisfaction of the condition (3.4). Let us emphasize that two parameters of the heat transfer simulation presented on *Fig. 11* by the curves *1* and *2* depend neither on a body shape nor on a model geometry. On the contrary, the equality of the two velocity gradients $V_s/R_m^*=V_\infty/R_N^*$ depends on subsonic and hypersonic flows geometry, shapes and dimensions of a body and a model.

In accordance with *Fig. 10*, along the Mars probe trajectory within the interval 25≤t≤44 s the velocity gradient at the shield stagnation point $\beta_{ef}=V_\infty(t)/R_N^*$ decreases monotonously in the range 4.4·10^3–3.2·10^3 s^{-1} for R_N=0.8 m and in the range 2.8·10^3–2.1·10^3 s^{-1} for R_N=1.25 m (see the curves *3* and *4* on *Fig. 11*).

Let's consider now the variation of the velocity gradient $\beta_{ep}=V_s(t)/R_m^*$ at the stagnation point of the euromodel (the cylindrical model of 50 mm in diameter with a flat face and the rounded edge of 11 mm in radius with R_m^*=3.2·10^{-2}m) if the parameters p_s and h_s change in the way, as *Fig. 11* requires.

It is very important to understand that in the plasmatron flow velocity V_s is not an independent parameter - it is definitely linked with the gas flow rate through the discharge channel Q, the enthalpy h_s and the pressure p_s. For further estimations we need to have some approximation for the dependence $V_s=V_s(Q,h_s,p_s)$. As a next step on the basis of the previous experimental and numerical data we assume the following approximation at pressures p_s<0.1 atm

$$V_s\left(h_s, p_s\right) = \frac{p_s^0}{p_s} V_s^0\left(h_s\right), \quad p_s^0 = 0.1 \text{ atm} \quad (7.1)$$

The experimental dependency $V_s^0(h_s)$ at the pressure 0.1 atm is taken from refs. 11, 12.

For the cylindrical model of 50 mm in diameter with the rounded edge of 11 mm in radius (the euromodel) and the subsonic flow configuration in the IPG-4 (R_c=40 mm) on the basis of the previous numerical solution of the Navier-Stokes equations [ref. 12] we have the following approximations for the velocity gradient and effective radius

$$\left(\frac{dU_{ep}}{dr}\right)_0 \cong 0.78\frac{V_s}{R_m}, \qquad (7.2)$$

$$R_m^* = 1.28R_m \cong 3.2\cdot 10^{-2}\ \text{m}$$

In *Fig. 11* the curve *5* shows the velocity gradient $\beta_{ep}(t)=V_s(t)/R_m^*$ that has been calculated from formula (7.2) taking into account (7.1) and dependencies $p_s(t)$and $h_s(t)$. We can see, that this velocity gradient $\beta_{ep}(t)$ decreases monotonously within the time interval $35\le t\le 44$ s from $4.7\cdot 10^3$ to $1.15\cdot 10^3$ s^{-1}. The curve *5* crosses the curves *3* and *4* at the points t=36.5 and 39.5 s.

That means that for the given value of the probe nose radius it is possible to duplicate in the IPG-4 plasmatron all three conditions (3.3), (3.4) for the one trajectory point only. For the nose radius R_N=0.8 m the point of the complete heat transfer simulation is: t_1=36.5 s, H=45.4 km, V_∞=5524 m/s (M_∞=28.9); the corresponding subsonic jet parameters are the following: p_s=5.8·10^{-2}atm and h_s^o=15.3 MJ/kg. For the nose radius R_N=1.25 m the desired point is: t_2=39.5 s, H=41.8 km, V_∞=5163 m/s (M_∞=26.7); the corresponding subsonic jet parameters are the following: p_s^o=7.8·10^{-2} atm and h_s^o=13.3 MJ/kg. We see that both points t_1 and t_2 are close to the point t^* where the heat flux has a maximum value and $t_1<t^*<t_2$. At these two trajectory points the stagnation point heat fluxes to the probe would be less than the maximum values of the heat fluxes but these differences would be within 1% (see *Fig. 10*). So, in fact, a remarkable opportunity for complete simulation of the heat transfer to the Mars probe quite close to the most important point of the entry into Martian atmosphere by using the IPG-4 plasmatron and the euromodel arises.

We should emphasize once more that partial duplication of only two parameters p_s and h_s along a trajectory in the real time scale would be not acceptable. In this way in test we shall have excessive heat fluxes if $t<t^o$ and underestimated heat fluxes if $t>t^o$, where $t^o=t_1$ if R_N=0.8 m and $t^o=t_2$ if R_N=1.25 m. Therefore, the most correct test technique for the study of the thermochemical resistance of the TPM for the vehicle during his entry into Martian atmosphere would be tests at constant values p_s^o and h_s^o during 15 s.

8. Prediction of Subsonic Carbon Dioxide Test for Mars Pathfinder

Let us consider another application of the LHTS concept to a prediction of the high-enthalpy test conditions in the IPG-4 plasmatron for precise simulation of the stagnation point heating for the Mars Pathfinder aeroshell which is a 70-deg sphere cone with a nose radius of 0.6625m [ref. 3]. In accordance with ref. 3 the maximum of the heat flux is achieved at the altitude 40.7 km and the following free stream conditions in the Martian atmosphere (C_{CO2}=0.97, and C_{N2}=0.03): V_∞=6590 m/s and ρ_∞=3.23·10^{-4} kg/m^3. The IPG-4 operating envelope for the subsonic regime with carbon dioxide as a working gas contains the peak-heating parts of the Mars Pathfinder [ref. 3] trajectory (*Fig. 9*).

The desired test conditions are determined for a subsonic dissociated carbon dioxide flow around the cylindrical model of 50 mm in diameter with a flat face and the rounded edge of 11 mm in radius which is supposed to be exposed for testing in the 100-kW IPG-4 plasmatron with the quartz discharge channel of 80 mm in diameter [refs. 11-14].

Now we can recalculate the entry parameters specified above to plasmatron test conditions by using formulae (3.3), (3.4) and (7.2). This simple technique (when the effective radius R_m^* is known) gives the following test conditions: the enthalpy H_e=21.73 MJ/kg, the static pressure p_s=0.14 atm, the flow velocity V_s=184 m/s. For the considered test configuration the calculated dimensionless parameters in equations (4.1) are: Δ=0.4, u_{1e}=0.39, α_e=2.10.

For these flow parameters and test geometry described above the stagnation point heat transfer rates have been calculated as a function of the surface temperature T_W and the effective catalytic efficiency γ_W from the numerical solution of the 1D boundary layer problem (4.1), (4.2) for a 5-species dissociated carbon dioxide mixture (CO_2, O_2, CO, O, and C).

The next assumptions have been made: 1) the following reactions are running in the mixture: $CO_2+M\leftrightarrow CO+O+M$, $O_2+M\leftrightarrow O+O+M$, $CO+M\leftrightarrow C+O+M$, $CO+O\leftrightarrow C+O_2$,, $CO_2+O\leftrightarrow CO+O_2$;, 2) the surface catalytic recombination of the CO molecules in the reaction $CO+O\rightarrow CO_2$ and O atoms in the reaction $O+O\rightarrow O_2$ are the reactions of the first order with equal efficiencies γ_W, and the C atoms are not involved in surface reactions. The same fourth-order-accurate finite-difference scheme was exploited for the numerical solution of the boundary layer problem (4.1), (4.2).

The computed stagnation point heat flux envelope for the predicted subsonic test is shown in *Fig. 12*. The upper border of this envelope (the curve *1*) corresponds to the fully catalytic surface (γ_W=1), the lower border (the curve *7*) - to the noncatalytic surface (γ_W=0). The

solid curves *2-6* correspond to the constant values of γ_W, $=10^{-1}$, $3\cdot10^{-2}$, 10^{-2}, $3\cdot10^{-3}$, 10^{-3}, the line *8* corresponds to the theoretical minimum of the heat flux from the frozen boundary layer to the noncatalytic wall.

The heat flux envelope is limited from the right side by the curve $q_W=\varepsilon_{th}\sigma T_W^4$, where ε_{th} is the total hemispherical emissivity, σ is the Stefan-Boltzmann constant. The curves *9* and *10* correspond to radiative-equilibrium walls with $\varepsilon_{th}=1$ and 0.78.

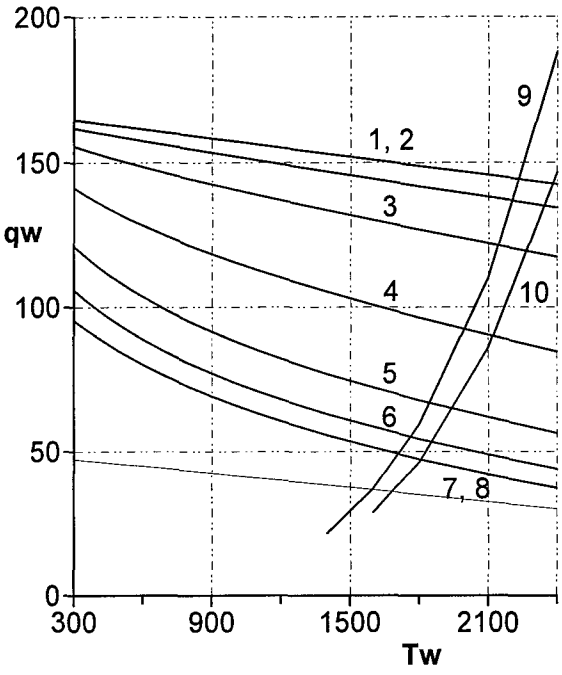

Fig. 12. Heat flux envelope for the IPG-4 plasmatron subsonic regime for the duplication of the stagnation point heat transfer to the Mars Pathfinder aeroshell (R_N=0.6625 m) at the peak-heating point (h=40.7 km, V_∞=6.59 km/s) by using an euromodel ($R_m=2.5\cdot10^{-2}$m).

Now it is very easy to determine the heat flux and the radiative-equilibrium surface temperature for the given values of ε_{th} and γ_W: q_W and T_W are just the coordinates of the intersection point for two curves - $q_W=q_W(T_W, \gamma_W=\text{const})$ and $q_W=\varepsilon_{th}\sigma T_W^4$. Thus, in the predicted test at ε_{th}=0.78 for the fully catalytic wall we have q_W=142 W/cm^2 and T_W=2380 K, for the noncatalytic wall - q_W=47 W/cm^2 and T_W= 1800 K.

For the heat transfer rates at the stagnation point of the Mars Pathfinder aeroshell and the radiative-equilibrium wall we have the maximum values q_W=127 W/cm^2 and T_W=2315 K at the wall condition of fully recombined CO_2 and q_W=42 W/cm^2 and T_W=1755 K in the non-catalytic wall case [ref. 3].

So, we observe quite sufficient agreement between the numerically predicted whole heat flux ranges for the Mars Pathfinder aeroshell at the trajectory peak-heating point and for test with an euromodel in the subsonic high-enthalpy carbon dioxide jet, which could be performed in the IPG-4 plasmatron with free stream parameters determined on the basis of the LHTS concept.

It is important that the enthalpy and pressure values determined above belong to the operating envelope of the IPG-4 plasmatron in a subsonic mode (*Fig. 9*) and the maximum of the thermochemical load on the stagnation point of the Pathfinder aeroshell could be duplicated precisely enough.

Recently it was shown in ref. 24 that quite precise duplication of the stagnation point heat flux to the Mars Probe [ref. 17] also could be achieved by using the IPG-4 plasmatron in subsonic regime with carbon dioxide as working gas.

This analysis was performed without taking into account the surface ablation, but in general the LHTS concept validated here can be applicable to a heat transfer problem with ablation effects if the influence of injection into the incoming flow is not very strong.

9. The Range of Applicability of the LHTS Concept

The derivation of conditions (2.7) - (2.9) of the local heat transfer simulation was based on the boundary layer theory and the assumption of local thermodynamic equilibrium in the subsonic flow (outside the boundary layer), which is fairly accurately satisfied for molecular gases (air, nitrogen, oxygen, carbon dioxide) in inductive plasmatrons at pressures $p\geq0.1$ atm.

It was found in ref. 25 that the boundary layer theory is applicable for calculating stagnation point heat transfer in subsonic high enthalpy flows at Reynolds numbers $Re_S = \rho_S V_S R_m^* / \mu_S \geq 30$, if the velocity gradient at the stagnation point on the model is determined with making allowance for the finite thickness of the boundary layer. Practically, for the models used in the heat transfer tests in the IPG plasmatrons $30<Re_S<3\cdot10^2$.

Thus, the general conditions of the LHTS concept formulated above are applicable for subsonic high enthalpy molecular gas flows in plasmatrons when $p\geq0.1$ atm and Re_S >30. For the surfaces with a high catalycity the LHTS concept is valid in the full range of the pressure, for the surfaces with moderate catalycity the lower border of the pressure range should be estimated. For the accurate computations of the velocity gradient or effective radius for subsonic test conditions the numerical solution of the Navier-Stokes equations must be used.

The accuracy of the prediction of ground test parameters or extrapolation to flight could be improved if the velocity gradient for flight conditions is calculated more accurately directly from the numerical solution of the hypersonic shock layer problem.

10. Comments to Thermochemical Simulation in Supersonic Tests

Traditionally, in high enthalpy tests practice, especially in tests performed by using arc-jet facilities, supersonic regimes are used more often, then subsonic ones. The LHTS concept gives us the strict inequalities for the similarity parameters ξ and ζ (see (2.10)), when supersonic high enthalpy flow should be performed for the providing of the correct duplication of the stagnation point heat transfer:

$$\frac{\sqrt{2H_\infty}}{V_\infty}\zeta_* \le \xi \le 1, \quad \zeta_* = \sqrt{\frac{\gamma_{*S}-1}{\gamma_{*S}+1}} \le \zeta \le 1 \qquad (10.1)$$

These inequalities mean that some supersonic test is necessary, if the nose radius and the model radius are comparable, although $R_m<R_N$: practically, for the simulation of the hypersonic heating of a vehicle with a small nose radius.

For the case of duplication of the heat transfer to a nose cap with small radius the simulation conditions for velocity and enthalpy (2.7) remain valid, but the conditions for pressure (2.8) must be modified. For supersonic simulating flow, in which the gas between the shock wave and the outer edge of the boundary layer near the flow axis is in the equilibrium state, this modification consists in the following. In the approximate Poisson adiabatic equation (2.5), applied to the equilibrium gas moving behind the shock, the pressure and Mach number are eliminated by means of the Rankine-Hugoniot conditions on the shock wave, and equations (2.7). As a result we obtain

$$\frac{p_S}{p_W} = \frac{(1-\zeta^2)(1-\varepsilon_S\zeta^2)^{\tau_{*Sh}}}{1+(2\tau_{*S}(1-\varepsilon_S)-1)\zeta^2}, \qquad (10.2)$$

$$\varepsilon_S = \frac{\rho_S}{\rho_{Sh}}, \qquad \tau_* = \frac{\gamma_*}{\gamma_*-1}$$

Where γ_* is the effective specific heat ratio, subscripts S and Sh relate to the parameters in the plasmatron free stream and behind the shock.

The validation of the conditions (2.7) and (10.2) as the basis of the LHTS concept for supersonic tests is not in fact yet, because the corresponding procedure requires the computations of the high enthalpy reacting supersonic flows in thermal and chemical nonequilibrium in the framework of the full Navier-Stokes equations.

11. Discussion

The accuracy of the prediction for the thermochemical action of the reacting gas on a vehicle surface for a hypersonic flight conditions, based on the LHTS concept, depends on the surface catalycity and the displacement of gas temperatures from the equilibrium values at the outer edges of the boundary layers on a body and a model. For surfaces with high and moderate catalycity the satisfaction of the conditions (3.3), (3.4) or (3.6) ensures the accurate duplication of the convective heat fluxes and the diffusive fluxes of atoms in subsonic high-enthalpy jets, when $R_m<<R_N$.

For the real TPM with catalytic efficiency $\gamma_W>>3\cdot10^{-3}$ the above mentioned conditions of a local heat transfer simulation can guarantee in test not only full-scale heat transfer rates, but real nonequilibrium chemistry within boundary layer as well. If the states of the dissociated gas flow at the edge of the boundary layer in the test or hypersonic flow conditions are significantly non-equilibrium, ground test parameters, predicted by using of the LHTS concept in order to simulate the heat transfer to a noncatalytic surface, may be applied as support values.

The LHTS concept makes an analysis of heat transfer parameters along trajectory rather simple and gives clear algorithm of the determination of the trajectory point for which stagnation point heat transfer could be accurately duplicated without taking into account the actual information about TPM catalycity.

As we have seen, the computed heat flux range for simulation of the stagnation point heat transfer rate to the Mars Pathfinder aeroshell at the trajectory peak-heating conditions in the subsonic high-enthalpy carbon dioxide flow is found in sufficient agreement with the study carried out through the full viscous shock layer computations in ref. 3.

Conclusion & Outlook

It is common knowledge now that modern ground facilities are unable to produce all flight conditions above Mach 8. At the same time the quantitative heat transfer could be duplicated in plasmatron quite precisely at least for a vehicle stagnation point. The LHTS concept reveals the new capabilities in the planning of a high-enthalpy experiment and the new approach to the extrapolation from ground to flight. For the complete stagnation point thermo-chemical simulation the triad of parameters - *total enthalpy-stagnation pressure-velocity gradient* - must be duplicated in a high-enthalpy test. In this kind of the heat transfer simulation the pairs of the parameters *M-Re* and *ρL-V* [ref. 26], which are widely used in aerodynamics, are not the similarity parameters in the stagnation point heat transfer.

The conditions of the hypersonic flow past a blunt body and the desired conditions of the free stream in ground test could be easily linked on the basis of the LHTS concept if one knows or can calculate an effective model radius by using CFD for the test configuration. For the typical entry trajectory, if the geometry of a model is specified, those conditions determine only one trajectory point, for which the complete local simulation could be achieved. If the trajectory point and the nose radius are

specified, conditions of the heat transfer duplication determine the test conditions and the effective radius of a model.

In the more dramatic noncatalytic surface case, we have to solve numerically not only the nonequilibrium shock layer problem for flight conditions, but also to compute the nonequilibrium plasma flow within a plasmatron discharge channel and a subsonic (or supersonic) reacting gas flow past a model for the prediction of the well-documented test conditions. So, CFD modeling is an indispensable tool for the construction of the bridge from ground test to flight and for the verification of the quality of flight parameters duplication in plasmatron tests. The interaction between ground testing and CFD modeling is a genesis for real gas effects duplication and extrapolation to flight.

Above examples of the LHTS concept applications clearly shown that the maximum thermochemical load on a vehicle surface at the stagnation point and TPM behavior can be directly duplicated for the wide range of the reentry and entry conditions in the Earth and the Martian atmospheres by using the inductive plasmatrons in the subsonic regimes.

Acknowledgements

The preparation of this paper was supported by RTA contract 4329A and the research has been performed in part under the INTAS-RFBR grant 95-1329 and the ISTC project 036. The author would like to express his gratitude to Prof. J.F. Wendt, Prof. M. Carbonaro and Prof. J.-M. Charbonnier for inviting to the VKI at the RTA/AVT Special Course, and to thank Dr. V.Shchelin for providing the shock layer parameters from his own code and Dr. S.Vasil'evskii for help in computations and figures design.

References

1. Kolesnikov, A.F., "Conditions of Simulation of Stagnation Point Heat Transfer from a High-Enthalpy Flow," Fluid Mechanics, Plenum, (tr. from Russian), v. 28, No. 1, 1993, p. 131.

2. Kolesnikov, A.F., "The Aerothermodynamic Simulation in Sub- and Supersonic High-Enthalpy Jets: Experiment and Theory," Proc. of the Second European Symposium on Aerothermodynamics for Space Vehicles, ESTEC, Noordwijk, The Netherlands, November 1994, ESA SP-367, 1995, p. 583.

3. Gupta,R.N., Lee, K.P., Scott, C.D., "Aerothermal Study of Mars Pathfinder Aeroshell," J. of Spacecraft and Rockets, 1996, v. 33, No. 1, p. 61.

4. Wendt, J.F., Muylaert, J.M., "Status of Hypersonic Testing Capabilities in Europe", Proc. of the Second European Symposium on Aerothermodynamics for Space Vehicles, ESTEC, Noordwijk, The Netherlands, November 1994, ESA SP-367, 1995, p. 165.

5. Anderson, L.A., "Effect of Surface Catalytic Activity on Stagnation-Point Heat Transfer Rates," AIAA J., 1973, No. 11, p. 649.

6. Scott, C.D., "Catalytic Recombination of Nitrogen and Oxygen on High Temperature Reusable Surface Insulation," Progress in Astronautics and Aeronautics, v. 77, edited by A.L. Crosbie, AIAA, New York, 1981, p. 192.

7. Vasil'evskii, S.A., Kolesnikov, A.F., Yakushin, M.I., "Determination of the Effective Probabilities of the Heterogeneous Recombination of Atoms When Heat Flow is Influenced by Gas-Phase Reactions," High Temperature, Plenum, (tr. from Russian), 1991, v. 29, No. 3, p. 411.

8. Stewart, D.A., Chen, Y., Bamford, D.J., Romanovsky, A.B., "Predicting Material Surface Catalytic Efficiency Using Arc-Jet Tests," 1995, AIAA 95-2013.

9. Gulhan, A., Vennemann, D., Yakushin, M., Zhestkov, B., "Comparative Oxidation Tests on Reference Material in Two Induction Heated Facilities," presented at the 46th International Astronautical Congress, Oslo, Norway, October 1995.

10. Eitelberg, G., Krek, R., Beck, W., "Stagnation Point Heat Transfer Testing in Non-Equilibrium Flow Produced by the HEG,"1996, AIAA 96-4504.

11. Bykova, N.G., Vasil'evskii, S.A., Gordeev, A.N., Kolesnikov, A.F., Pershin, I.S., Yakushin, M.I., "An Induction Plasmatron Application for Simulation of Entry into Martian Atmosphere," Proc. of the Third International Symposium on Environmental Testing for Space Programmes, ESTEC, Noordwijk, The Netherlands, June 1997, ESA SP-408, p. 195.

12. Bykova, N.G., Vasil'evskii, S.A., Gordeev, A.N., Kolesnikov, A.F., Pershin, I.S., Yakushin, M.I., "Determination of the Effective Probabilities of Catalytic Reactions on the Surfaces of Heat Shield Materials in Dissociated Carbon Dioxide Flows," Fluid Mechanics, Plenum, (tr. from Russian), 1997, v. 32, No. 6, p. 876.

13. Kolesnikov, A.F., Pershin, I.S., Vasil'evskii, S.A., Yakushin, M.I., "Study of Quartz Surface Catalycity in Dissociated Carbon Dioxide Subsonic Flows," 1998, AIAA 98-2847.

14. Kolesnikov, A., Yakushin, M., Vasil'evskii, S., Pershin, I., and Gordeev, A. "Catalysis Effects on Quartz Surface in High-Enthalpy Oxygen & Carbon Dioxide Flows", 3rd European Symposium on Aerothermodynamics for Space Vehicles, ESTEC, Noordwijk, The Netherlands, 24-26 November 1998, ESA SP-426, 1999, p. 537.

15. Lozino-Lozinskii, G. E., "Buran Flight," in: Gagarin Scientific Studies in Aviation and Cosmonautics, 1989 (in Russian), Nauka, Moscow, 1990, p. 6.

16. Voinov, L.P., Zalogin, G.N., Lunev, V.V., Timoshenko, V.P., "Comparative Analysis of Laboratory and Full- Scale Data Concerning "Bor" and "Buran" Space Vehicles Thermal Protection Material Catalycity," Cosmonautics and Rocket Engineering, TSNIIMASH, (in Russian), 1994, No. 2, p. 51.

17. Rubio Garcia, V., Marraffa, L., Scoon, G., Roumeas, R., "Mars Mini-Probes. Elements of Aerothermo-dynamics & Entry Trajectories," 3rd European Symposium on Aerothermo- dynamics for Space Vehicles, ESTEC, Noordwijk, The Netherlands, 24-26 November 1998, ESA SP-426, 1999, p. 155.

18. Fay, J. A. and Riddell, F. R., "Theory of Stagnation Point Heat Transfer in Dissociated Air," J. Aeronaut. Sci., 1958, v. 25, No. 2, p. 73.

19. Goulard, R., "On Catalytic Recombination Rates in Hypersonic Stagnation Heat Transfer," Jet Propulsion, 1958, v. 28, No. 11, p. 737.

20. Lunev, V.V. Hypersonic Aerodynamics, (in Russian), Moscow, Maschinostroenie, 1975, 328 p.

21. Kolesnikov, A.F. and Yakushin, M.I., "Determination of Heterogeneous Recombination Effective Probabilities of Atoms from Heat Fluxes to the Surface in Dissociated Air Flow," Matematicheskoe Modelirovanie (in Russian), 1989, v. 1, No. 3, p.44.

22. Vasil'evskii, S.A., Kolesnikov, A.F., Yakushin, M.I., "Mathematical Models for Plasma and Gas Flows in Induction Plasmatrons," Molecular Physics and Hypersonic Flows, ed. by M.Capitelli, NATO ASI Series, v. 482, Kluwer, 1996, p. 495.

23. Kolesnikov, A.F., Shchelin, V.S., "Numerical Analysis of Simulation Accuracy for Hypersonic Heat Transfer in Subsonic Jets of Dissociated Nitrogen," Fluid Dynamics, Plenum, (tr. from Russian), 1990, v. 25, No. 2, p.278.

24. Kolesnikov, A., Marraffa L., "An Analysis of Stagnation Point Thermochemical Simulation by Plasmatron for Mars Probe," 1999, AIAA 99-3564.

25. Kolesnikov, A.F., Yakushin, M.I., "Modeling of Convective Nonequilibrium Heat Transfer for Bodies in Hypersonic Flows by Plasmatrons," High Temperature, Plenum, (tr. from Russian), 1988, v. 26, No. 4, p. 569.

26. Vennemann, D., "Hypersonic Aerodynamic/Aero-thermal Test Facilities available in Europe to support Space Vehicle Design," AGARD Symposium on Space Systems Design and Development Testing, Cannes, France, Oct. 1994.